Monitoring the Lithium Concentration across the Thickness of Silicon-Graphite Electrodes during the First (De-)Lithiation

Monitoring the Lithium Concentration across the Thickness of Silicon-Graphite Electrodes during the First (De-)Lithiation

Morten Wetjen,[1,=,z] Markus Trunk,[2,=] Lukas Werner,[2] Hubert A. Gasteiger,[1,*] Roman Gernhäuser,[3] Ralph Gilles,[4] Bastian Märkisch,[2] and Zsolt Révay[4]

[1] *Chair of Technical Electrochemistry, Department of Chemistry and Catalysis Research Center, Technische Universität München, D-85748 Garching, Germany*
[2] *Professorship of Fundamental Particle Physics at Low Energies, Physics Department, Technische Universität München, D-85748 Garching, Germany*
[3] *Central Technology Lab, Physics Department, Technische Universität München, D-85748 Garching, Germany*
[4] *Heinz Maier-Leibnitz Zentrum (MLZ), Technische Universität München, D-85748 Garching, Germany*

Progressing from graphite to silicon-based anodes for lithium-ion batteries increases the importance of a depth-resolved understanding of the reversible and irreversible processes across the thickness of the anode electrode. Considerable changes in electrode volume and mass loading upon (de–)lithiation make silicon electrodes more susceptible to continuous side reactions and to the isolation of active material particles, leading to non-uniform and accelerated electrode degradation. Here, we investigate the evolution of lithium concentration profiles across the thickness of porous silicon-graphite (SiG) electrodes (~20 µm thickness, ~1.7 mAh cm^{-2}) with 35 wt% silicon nanoparticles during the first (de–)lithiation cycle. Using ex situ neutron depth profiling (NDP), we monitor depth- and quantity-resolved (i) the solid-electrolyte-interphase (SEI) formation, (ii) the (de–)lithiation of the active materials, as well as (iii) the changes in the total lithium content as a function of the state-of-charge (SOC) and depth-of-discharge (DOD). The results provide depth–resolved information about reversible and irreversible processes occurring during the formation of SiG electrodes, and thus offer insight into the formation process of silicon-based electrodes.
 [DOI: 10.1149/2.0581908jes]

Manuscript submitted January 7, 2019; revised manuscript received April 14, 2019. Published April 29, 2019.

The commercialization of lithium-ion batteries featuring high-capacity silicon-based anodes has been hampered by severe degradation phenomena of the silicon particles and the respective electrode coatings.[1–3] Silicon particles undergo significant morphological changes upon (de–)lithiation, which result in an ongoing decomposition of electrolyte constituents.[4,5] On an electrode-level, this leads to a considerable increase of the mass loading and to concomitant swelling of the electrode[6,7] that deteriorates interparticle contacts and also the ion conducting pathways.[3,8] Consequently, silicon electrodes are highly susceptible to non-uniform active material utilization and isolation of active material particles. To understand in more detail the underlying reversible and irreversible processes requires a depth-resolved quantification of the lithium concentration across the electrode thickness.

Neutron depth profiling (NDP) is a nuclear analytical technique which is highly sensitive to ^{6}Li and thus allows to measure the distribution of lithium across the thickness of battery electrodes.[9,10] Although the detectable depth strongly depends on the electrode mass loading and its elemental composition, practically relevant silicon-graphite electrodes can typically be investigated up to thicknesses of ~50 µm.[11] Furthermore, the method is independent of the chemical state of the ^{6}Li isotopes, thus providing combined information stemming from all lithium-containing compounds in the investigated electrodes, including the binder, the SEI (solid electrolyte interphase), and the lithiated active materials.[12–14]

Experimental

Silicon-graphite (SiG) electrodes, consisting of 35 wt% silicon nanoparticles (~200 nm, Wacker Chemie AG, Germany), 45 wt% graphite (~20 µm, T311, SGL Carbon, Germany), 10 wt% vapor grown carbon fibers (VGCF-H, Showa Denko, Japan), and 10 wt% lithium poly(acrylate) binder (LiPAA)[15] were prepared by an aqueous ink procedure.[3] The electrode mass loading was adjusted to 1.41 ± 0.02 mg cm^{-2}, yielding a first-cycle delithiation capacity of 1.71 ± 0.03 mAh cm^{-2} at a C-rate of 0.1 h^{-1} (≈ 0.17 mA cm^{-2}) compared to a theoretical capacity of 2.00 ± 0.03 mAh cm^{-2}.[12]

Galvanostatic (de-)lithiation of the SiG electrodes to different SOC and DOD was conducted in Li//SiG coin-cells (Hohsen, Japan) at 0.1 h^{-1}. These were composed of a 20 µm thick polyolefin separator (Celgard, USA) and a 250 µm thick glass fiber separator (VWR, USA) sandwiched between a SiG electrode (Ø 14 mm) and a lithium metal electrode (Ø 15 mm, ~450 µm thickness, Rockwood Lithium, USA). As electrolyte, 1 M $LiPF_6$ in a mixture of fluoroethylene carbonate:ethyl methyl carbonate (FEC:EMC, 20:80 vol%, BASF, Germany) was used. To form an initial SEI, the first lithiation cycle starting from the open-circuit voltage (OCV) was stopped at 0.25 V vs. Li$^+$/Li; nominally 100%$_{SOC}$ were obtained by continuing to 0.01 V vs. Li$^+$/Li, while nominally 100%$_{DOD}$ were obtained by conducting the first delithiation cycle up to 1.5 V vs Li$^+$/Li. For all other SOC and DOD values, a capacity-cutoff was applied in 20% intervals of the first cycle reversible delithiation capacity of ~1.7 mAh cm^{-2} (i.e., in intervals of ~0.34 mAh cm^{-2}). The measurements were performed in a climate chamber (Binder, Germany) at 25°C, using a Maccor Battery Cycler 4000 (Maccor, USA).

After (de–)lithiation to defined SOC and DOD, the cells with SiG electrodes cycled to different potentials/capacities were immediately transferred into an argon-filled glove box (H_2O and O_2 concentration <0.1 ppm; MBraun, Germany). There, the SiG electrodes were extracted and carefully washed with dimethyl carbonate (DMC) to remove residues of the liquid electrolyte, thus slowing down relaxation of possible concentration gradients in the solid phase across the thickness of the electrode coating. The dry electrodes were then sealed in pouch foil and were only taken out just before the transfer into the NDP vacuum chamber. This limited their exposure to ambient air to a few minutes in order to mitigate side reactions. Nevertheless, it is not expected that side reactions would affect the lithium depth profile information, because they would only change the chemical state but not the location of the detected ^{6}Li isotopes (either intercalated or trapped in the SEI). In total, a time of less than 24 h was kept between the electrochemical (de–)lithiation and the NDP investigation in order to minimize the possible relaxation of lithium concentration gradients across

[=] These authors contributed equally to this work.
[*] Electrochemical Society Fellow.
[z] E-mail: morten.wetjen@tum.de

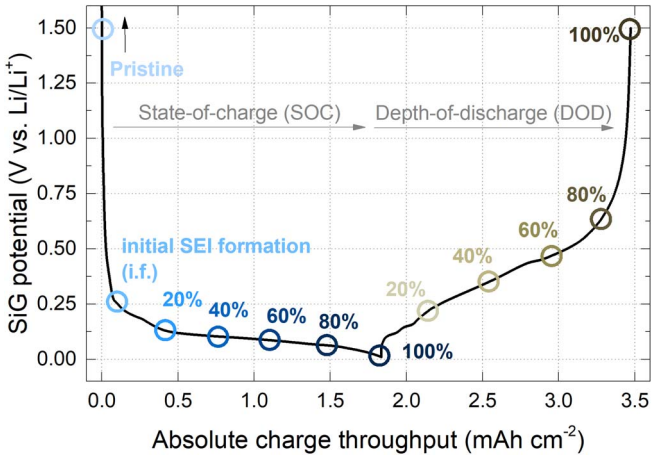

Figure 1. Galvanostatic potential profile of the first (de–)lithiation of the SiG electrodes in Li//SiG coin-cells at 0.1 h^{-1}. The open circles indicate the different SOC (blue) and DOD (brown) at which the SiG electrodes were harvested from the cells and measured by NDP. Additionally, an electrode cycled only to 0.2 V vs. Li^+/Li where the initial SEI formation (i.f.) occurs without lithiation is shown.

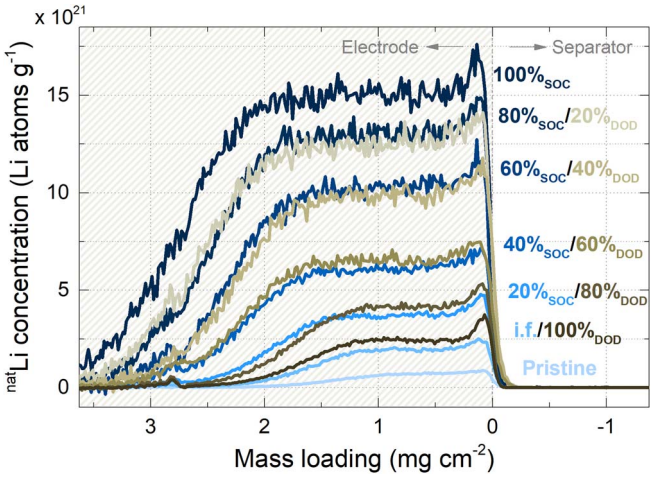

Figure 2. Lithium concentration profiles as a function of the SiG electrode mass loading which were calculated from the NDP energy spectra after (de-)lithiation to different SOC (blue) and DOD (brown).

the electrode thickness. The NDP measurements were conducted ex situ using the N4DP setup at the PGAA facility of MLZ in Garching, Germany.[11,16] The beamline provides a collimated cold neutron beam with an area of 12.6 mm^2 and a flux of 1.35×10^9 cm^{-2} s^{-1}.[17] The SiG electrodes were measured with the coating facing the incoming beam at an angle of 45°.

Results and Discussion

Electrochemical (de-)lithiation of SiG electrodes.—Figure 1 shows the galvanostatic potential profile of the first (de–)lithiation of the SiG electrodes as a function of the absolute charge throughput ($\equiv Q_{lithiation} + Q_{delithiation}$) at a rate of 0.1 h^{-1}. While the lithiation potentials of initially crystalline silicon and graphite largely overlap, the delithiation of graphite takes place at lower potentials (<0.2 V vs. Li^+/Li) compared to silicon.[3] However, since graphite accounts for only ~12% of the electrode's capacity,[6] the electrochemical behavior of the SiG electrodes is mainly influenced by the silicon particles. Accordingly, the lithiation is characterized by a large potential plateau around 0.1 V vs. Li^+/Li which can be ascribed to the two-phase amorphization of the initially crystalline silicon particles upon the alloy formation with lithium. The following delithiation shows a much more sloped profile which originates from dealloying of amorphous Li_xSi via a solid solution reaction. The small plateau around 0.45 V vs. Li^+/Li (between 40–60%DOD in Figure 1) indicates that only a minor fraction of the Li_xSi alloy has recrystallized at potentials below 0.05 V vs. Li^+/Li during the preceding lithiation to form the highly lithiated $Li_{15}Si_4$ phase.[18]

For the NDP measurements, a series of pristine SiG electrodes were (de–)lithiated to different SOC (blue circles) and DOD (brown circles) values. Besides fully lithiated ($100\%_{SOC}$) and fully delithiated ($100\%_{DOD}$) SiG electrodes, samples were taken in SOC/DOD intervals of 20% (viz., ~0.34 mAh cm^{-2}) during the first (de–)lithiation. In addition, two SiG electrodes in pristine state and after the initial SEI formation between OCV and 0.25 V vs. Li^+/Li were prepared as reference.

Lithium concentration profiles.—The nuclear reaction of thermal neutrons with ^{6}Li results in the formation of a ^{3}H particle (2727 keV) and a ^{4}He particle (2055 keV) with well-defined energies. Due to the two-body kinematics, the particles are emitted back-to-back whereby the residual energy of the particles can be used to determine the depth of the location of the original ^{6}Li isotope.[19] Figure 2 shows the lithium concentration profile as a function of the mass loading for the SiG electrodes at different SOC (blue lines) and DOD (brown lines). Following a procedure reported by Trunk et al.,[11] the lithium concentration and the mass loading were calculated from the ^{3}H energy spectra. First, the ^{4}He signal was mathematically subtracted from the ^{3}H signal because both signals arise from the same lithium profile.[11] Then, the ^{3}H intensity was converted into an absolute lithium quantity by normalizing the measured count rate using a reference material[20] and assuming a constant natural lithium abundance (7.59% for ^{6}Li). The electrode mass loading was calculated from the signal broadening due to the energy loss of the ^{3}H particles using the SRIM (stopping range in matter) software.[21] Because the energy loss is dependent on the material composition, changes in the stoichiometry of the SiG electrodes upon (de-)lithiation were also taken into account.

This was based on three different mass contributions: (i) The elemental composition of the pristine SiG electrodes ($m_{pristine}$), as described in the experimental section. (ii) The mass equivalent of the lithium content in the SiG electrode (m_{Li}), which was obtained from the net charge passed through the electrode Q_{net} ($\equiv Q_{lithiation} - Q_{delithiation}$) for each SOC/DOD, assuming every transferred electron corresponds to one lithium atom irrespective if it is inserted into the active material or part of the SEI ($m_{Li} = \frac{Q_{net} \cdot 6.941\ g\ mol^{-1}}{1 \cdot 96485\ As\ mol^{-1}}$). (iii) The residual mass of the other SEI compounds (excl. lithium), which was obtained by weighing the harvested electrodes and subtracting $m_{pristine}$ and m_{Li}. The corresponding stoichiometry was approximated by the FEC molecule m_{FEC} ($C_3H_3O_3F$), which is preferentially reduced on silicon electrodes.[4] Because no further information concerning the depth-dependent variation of the SiG electrode matrix-material are accessible, for the energy loss calculations it was approximated that changes in the electrode stoichiometry occur evenly across the entire electrode at the different SOC and DOD states.[12]

The lithium concentration profiles shown in Figure 2 can be read from the right to the left. A mass loading of zero marks the electrode/separator interface, while an increasing mass loading corresponds to greater electrode depth. Because the energy loss is a statistical process, the signal broadens toward higher mass loadings (≡ lower energies, originating from greater depth), whereby the inflection point indicates the interface between the SiG electrode and the Cu current collector.[11] In the pristine SiG electrode (lowest blue line), a small lithium concentration can be observed. This corresponds entirely to the LiPAA binder which is uniformly distributed across the SiG electrode thickness.[12] After the initial SEI formation at 0.25 V vs. Li^+/Li (blue line labelled "i.f."), the lithium concentration increases notably. Since the lithiation of crystalline silicon does

not occur at potentials above 0.25 V vs. Li^+/Li,[6] most of the absolute charge throughput (~0.13 mAh cm^{-2}, see Figure 1) can be ascribed to the reductive decomposition of electrolyte constituents, preferentially FEC,[4] and the subsequent formation of lithium-containing SEI compounds like LiF and Li_2CO_3. Upon continued lithiation of the SiG electrodes (blue lines), the lithium concentration increases steadily, which can be mostly attributed to the lithium intercalation into graphite (LiC_x) and the alloying with silicon (Li_xSi). In addition, the profile broadens toward higher mass loadings, which is caused by the large molar quantity of lithium as well as by the ongoing deposition of electrolyte decomposition products. For example, at $80\%_{SOC}$ the SiG electrode contains a capacity of ~1.44 mAh cm^{-2}. Using Faraday's law and assuming one electron per lithium, this translates into a lithium mass of 0.37 mg_{Li} cm^{-2}. Considering that this SiG electrode weighed 1.41 mg cm^{-2} in its pristine state and 1.93 mg cm^{-2} after cell disassembly, this corresponds to a mass increase of 0.52 mg cm^{-2} of which 0.37 mg_{Li} cm^{-2} account for lithium. The remaining 0.15 mg cm^{-2} can be ascribed to electrolyte decomposition products. Overall, the electrode mass loading increased by ~40% compared to the pristine state, resulting in a larger energy loss and a broadening of the lithium concentration profile. Remarkably, the plateau-like shape of the profiles in Figure 2 remains almost unchanged at different SOC/DOD and mass loadings, respectively, thus indicating a uniform lithium distribution across the thickness of the SiG electrode. Consequently, the lithiation of the active materials occurs homogeneously throughout the thickness of the SiG electrodes, which is consistent with the expected absence of lithium ion concentration gradients in the electrolyte phase within the pores of the only ~20 µm thick SiG electrodes at the low C–rate of 0.1 h^{-1}.[12]

Another feature in the concentration profiles is a small peak at the interface between the electrode and the separator, i.e., at the onset of the mass loading scale in Figure 2, which occurs independently of the individual SOC and DOD states. These findings corroborate to our earlier studies where the peak was found to vanish only after extensive charge-discharge cycling.[12] Although this phenomenon is still subject to further investigation, Trunk et al. reported earlier,[11] that it is not necessarily related to a true enrichment of lithium at the surface. Instead, they ascribed its origin to the solid-particle nature (e.g., particle size distribution) of the electrode coating, which results in a higher apparent amount of lithium-containing compounds in the outermost electrode layer compared to an average layer in the electrode bulk.

During the subsequent delithiation cycle, the lithium content and the mass loading decrease gradually, while the plateau-like profile is maintained at all DOD levels. Thus, the lithium deintercalation from LiC_x (mainly between $100\%_{SOC}$ and $80\%_{DOD}$) as well as the subsequent dealloying of Li_xSi occur homogeneously throughout the thickness of the electrode, analogous to what was observed during lithiation. Consequently, any immobilized lithium or electrolyte decomposition products are also uniformly distributed across the thickness of the electrodes. This becomes even more evident by comparing the SiG electrode after the initial SEI formation (labelled "i.f.") and the fully delithiated SiG electrode at $100\%_{DOD}$ (lowest brown line). Accordingly, both electrodes indicate the same profile shape and a similar lithium content; the slightly larger lithium concentration at $100\%_{DOD}$ can be attributed to ongoing SEI growth caused by silicon particle expansion and contraction over the course of the first (de–)lithiation cycle as well as a minor fraction of immobilized lithium trapped by electrically isolated active material particles. Thus, our results demonstrate that the here investigated SiG electrodes are uniformly (de–)lithiated at 0.1 h^{-1}, despite a considerable but mostly reversible change in the electrode mass loading of more than +50% (0.7–0.8 mg cm^{-2}) at $100\%_{SOC}$.

Quantifying the lithium content.—To verify that the lithium concentration profiles represent the entire SiG electrode, Figure 3 compares the total lithium content of the SiG electrodes vs. the absolute charge throughput by two different approaches: i) either calculated from the NDP spectra (open triangles) or ii) determined electrochemically by considering the net charge passed through the electrode Q_{net} ($\equiv Q_{lithiation} - Q_{delithiation}$), which was obtained from the electrochemical data (solid squares). The former were corrected by the lithium content measured for the LiPAA binder which cannot be determined from the electrochemical data. Accordingly, the integration of the ^3H signal from the NDP spectrum of the pristine SiG electrode reveals a lithium content of 0.049 ± 0.002 mAh cm^{-2}. This value agrees well with the ~0.048 mAh cm^{-2} derived from the composition of the pristine electrode, assuming an electrode mass loading of 1.41 mg cm^{-2}, 10wt% binder, and a molecular weight of 77.9 g mol^{-1} (i.e., the molecular weight of one repeat unit of LiPAA). As can be seen, throughout the first (de–)lithiation of the SiG electrode, the agreement between the electrochemically and the NDP–derived lithium content is excellent for all SOC and DOD values. This confirms that the lithium concentration profiles in Figure 2 indeed reflect the entire electrode coating and thus provide depth–resolved information about several reversible and irreversible processes, including the SEI formation, (de–)lithiation of the active materials, as well as the considerable changes in the electrode mass loading.

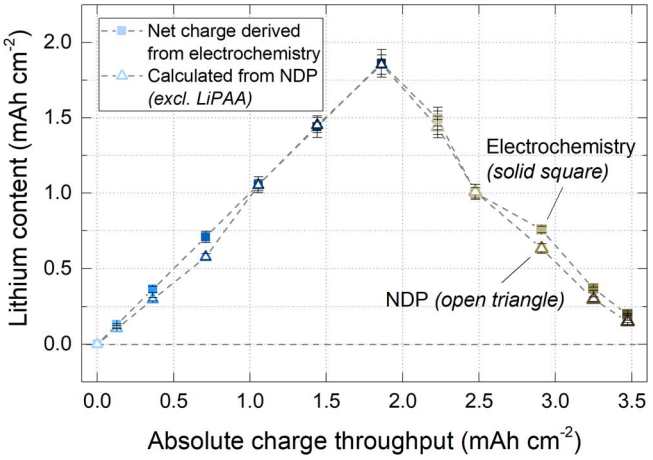

Figure 3. Total lithium content of the SiG electrodes as a function of the absolute charge throughput over the course of the first (de–)lithiation cycle to different SOC (blue) and DOD (brown) values. The lithium contents were either derived electrochemically from the net charge passed through the electrode (solid squares) or calculated from the NDP spectra (open triangles). The lithium content in the LiPAA binder was subtracted from the NDP data (0.049 mAh cm^{-2}) because it is not accessible from the electrochemical data.

Conclusions

Using ex situ NDP, we quantified the evolution of lithium concentration profiles across the thickness of SiG electrodes over the first (de–)lithiation cycle. Our results revealed that during the first (de-)lithiation at a slow C-rate of 0.1 h^{-1} both the initial SEI formation above 0.25 V vs. Li^+/Li as well as the ongoing electrolyte decomposition measured after full delithiation ($100\%_{DOD}$) occur uniformly across the thickness of the SiG electrodes. Despite considerable changes in the total lithium content and the electrode mass loading, the same plateau-like profile was maintained throughout the first (de–)lithiation cycle, thus indicating a depth-independent utilization of the active materials. A comparison of the lithium content determined from the electrochemical data and calculated from the NDP spectra revealed an excellent agreement. Therefore, NDP offers a powerful tool to evaluate various degradation phenomena of silicon electrodes in a depth-resolved way, including (i) the uniformity of the SEI growth upon cycling, (ii) the active material utilization in prelithiated or capacitively oversized silicon electrodes, as well as (iii) the SOC distribution at different C–rates.

Acknowledgments

Wacker Chemie AG is kindly acknowledged for providing the silicon nanoparticles. The Heinz Maier-Leibnitz Zentrum (MLZ) is kindly acknowledged for the possibility to use the high-quality neutron beam at the PGAA facility. The BMBF projects 05K16WO1 ("N4DP") and 03XP0081 ("ExZellTUM II") are gratefully acknowledged for financial support.

ORCID

Morten Wetjen https://orcid.org/0000-0002-2357-1151

References

1. M. N. Obrovac and V. L. Chevrier, *Chem. Rev.*, **114**, 11444 (2014).
2. D. Andre, H. Hain, P. Lamp, F. Maglia, and B. Stiaszny, *J. Mater. Chem. A*, **5**, 17174 (2017).
3. M. Wetjen, D. Pritzl, R. Jung, S. Solchenbach, R. Ghadimi, and H. A. Gasteiger, *J. Electrochem. Soc.*, **164**(12), A2840 (2017).
4. R. Jung, M. Metzger, D. Haering, S. Solchenbach, C. Marino, N. Tsiouvaras, C. Stinner, and H. A. Gasteiger, *J. Electrochem. Soc.*, **163**(8), A1705 (2016).
5. R. Petibon, V. Chevrier, C. P. Aiken, D. S. Hall, S. Hyatt, R. Shunmugasundaram, and J. R. Dahn, *J. Electrochem. Soc.*, **163**(7), A1146 (2016).
6. M. Wetjen, S. Solchenbach, D. Pritzl, J. Hou, V. Tileli, and H. A. Gasteiger, *J. Electrochem. Soc.*, **165**(7), A1503 (2018).
7. D. Mazouzi, N. Delpuech, Y. Oumellal, M. Gauthier, M. Cerbelaud, J. Gaubicher, N. Dupré, P. Moreau, D. Guyomard, L. Roué, and B. Lestriez, *J. Power Sources*, **220**, 180 (2012).
8. T. Yoon, C. C. Nguyen, D. M. Seo, and B. L. Lucht, *J. Electrochem. Soc.*, **162**(12), A2325 (2015).
9. S. M. Whitney, S. R. F. Biegalski, and G. Downing, *J. Radioanal. Nucl. Chem.*, **282**, 173 (2009).
10. S. C. Nagpure, P. Mulligan, M. Canova, and L. R. Cao, *J. Power Sources*, **248**, 489 (2014).
11. M. Trunk, M. Wetjen, L. Werner, R. Gernhäuser, B. Märkisch, Z. Révay, H. A. Gasteiger, and R. Gilles, *Mater. Charact.*, **146**, 127 (2018).
12. M. Wetjen, M. Trunk, L. Werner, R. Gernhäuser, B. Märkisch, Z. Révay, R. Gilles, and H. A. Gasteiger, *J. Electrochem. Soc.*, **165**(10), A2340 (2018).
13. X. Zhang, T. W. Verhallen, F. Labohm, and M. Wagemaker, *Adv. Energy Mater.*, 1500498 (2015).
14. D. X. Liu, J. Wang, K. Pan, J. Qiu, M. Canova, L. R. Cao, and A. C. Co, *Angew. Chemie - Int. Ed.*, **53**, 9498 (2014).
15. V. L. Chevrier, L. Liu, D. B. Le, J. Lund, B. Molla, K. Reimer, L. J. Krause, L. D. Jensen, E. Figgemeier, and K. W. Eberman, *J. Electrochem. Soc.*, **161**(5), A783 (2014).
16. L. Werner, M. Trunk, R. Gernhäuser, R. Gilles, B. Märkisch, and Z. Revay, *Nucl. Inst. Methods Phys. Res. A*, **911**, 30 (2018).
17. Z. Révay, P. Kudějová, K. Kleszcz, S. Söllradl, and C. Genreith, *Nucl. Instruments Methods Phys. Res. Sect. A*, **799**, 114 (2015).
18. M. N. Obrovac and L. Christensen, *Electrochem. Solid-State Lett.*, **7**(5), A93 (2004).
19. J. P. Biersack, D. Fink, R. Henkelmann, and K. Müller, *Nucl. Instruments Methods*, **149**, 93 (1978).
20. NIST. *Certificate of Analysis Standard Reference Material* 2137, (2010).
21. J. F. Ziegler, M. D. Ziegler, and J. P. Biersack, *Nucl. Instruments Methods Phys. Res. Sect. B*, **268**, 1818 (2010).